ELSEVIER

Chemical Engineering Journal 66 (1997) 159–169

Chemical Engineering Journal

Experimental study of a finned tubes impact gas–solid separator for CFB boilers

Kefa Cen *, Xiaodong Li, Yangxin Li, Jianhua Yan, Yueliang Shen, Shaorong Liang, Mingjiang Ni

Institute for Thermal Power Engineering, Zhejiang University, 310027 Hangzhou, People's Republic of China

Received 10 May 1995; accepted 17 October 1996

Abstract

We present a finned tubes impact gas–solid separator with enhancing heat transfer behavior which can be used in circulating fluidized bed boilers (CFBB). Experimental results show that this separator has advantages such as high separation efficiency, low pressure drop and compact structure. Furthermore, it can also enhance heat transfer, and fins welded on the tubes can be cooled at the same time by the work medium in the tubes so that they can be made by common boiler steel. We describe the fluid dynamics characteristics, heat transfer and separation performance of the finned tubes separator through a series of experiments. © 1997 Elsevier Science S.A.

Keywords: Impact separation; Fluid dynamics; Fluidized bed; Boiler

1. Introduction

Worldwide attention is now paid to the development of clean coal combustion technologies. Among these technologies, circulating fluidized bed combustion (CFBC), which has been widely applied, has good characteristics such as satisfactory desulfurization efficiency, combustion efficiency, low NO_x emission, suitability for different types of coal, good performance for control and appropriate capital and operation costs.

As key equipment for circulating fluidized bed boilers (CFBB), gas–solid separators, which help the circulation of the solids in the furnace, have strong effects on the combustion efficiency, the circulation rate, the desulfurization efficiency, and so on. At present, cyclones are the most widely used separators in CFBB. Although used for a long time and having high efficiency, cyclones have disadvantages such as high pressure drop (~2 kPa), serious wear, high thermal inertia, and long start-up and cool-down times. An especially serious problem is that the size of hot cyclones increases rapidly with the capacity of CFBB; for example, the diameter of some commercial cyclones reaches 10 m [1] thus making them almost as large as the furnaces of the boilers. Large cyclones also result in some manufacturing, installation and operation problems. Therefore, it is essential to develop new types of gas–solid separators that should have high efficiency, low pressure drop and compact structure, and so on.

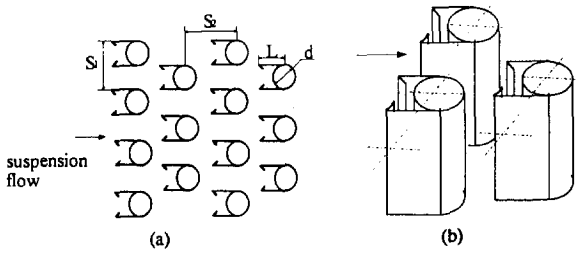

Fig. 1. Targets of the finned tubes impact separator.

Compared with cyclones, inertial separators have low pressure drop, compact structure and low capital cost, and their application in CFBB is now paid great attention, for example the U-beams separator of Sweden's Studsvik Corporation [2,3], the slots separator of Germany's Steinmuller Corporation [4], and the slotted-tube impact separator of China's Xi'an Jiaotong University [5]. These separators have shown that the separation efficiency of inertial separators can, to some extent, meet the demand of some CFBB.

The above mentioned inertial separators do not combine separation with heat transfer. This paper puts forward a new type of finned tubes impact gas–solid separator with enhancing heat transfer behavior [6]. Targets of this separator (see Fig. 1) are superheated or convective tubes welded with shaped fins, thus also improving the heat transfer behavior of

* Corresponding author.

PII S1385-8947(96)03179-8

the tubes. Flow stagnant regions are created in the slots between pairs of fins. When passing through the targets, the suspension impacts on the targets and repeatedly changes its flow path. Because of inertia, the particles that have a larger momentum than that of the gas can be separated from the main gas stream. When entering the flow stagnant regions, the particles may fall down along the slots to the ash hopper. Moreover, the fins can be cooled by the work medium in the tubes so that fins made of common boiler steel can be used in high temperature conditions. With the support of the tube, it will be difficult to change the shape of the fin when the fin's length is too long along the tube, which is one of the features of the separator.

This paper presents the fluid dynamics characteristics of finned tubes measured by means of a laser Doppler velocimeter (LDV) for a single phase and a particle dynamics analyzer (PDA) for two phases, and the heat transfer characteristics of the fin. Based on this study, cold model experiments for separation and pressure drop performance of the separator have been carried out and some optimum design parameters are obtained.

2. Fluid dynamics characteristics of finned tubes

A laser Doppler velocimeter (LDV) made by American TSI Co. was used to measure the flow structure of a single finned tube. Fig. 2 shows the LDV measurement system. A finned tube is placed horizontally in the measuring part which is a Plexiglas® square-cross-sectional pipe. The flow rate of the gas fed into the pipe is 102 $m^3 h^{-1}$, and the inlet velocity is 4.2 m s^{-1}. By measuring the velocity of the tracer loaded in the gas, the velocity and turbulent intensity of the gas phase are obtained [7]. The coordinate systems of the measurement parts are shown in Fig. 3.

A three-dimensional particle dynamics analyzer equipped with a He : Ne laser with a maximum power of 10 W (Dantec Measurement Technology A/S) was adopted to measure the two-phase fluid dynamics characteristics of a single tube and finned tubes. Fig. 4 shows the PDA measurement system. The particle tracers are white resin. The flow rate of the gas was the same as that of the LDV. The particle concentration ranged from 0.17 to 0.44 kg m^{-3}. The coordinate systems are also shown in Fig. 3.

Fig. 5 shows the velocity distribution of the gas in the x-direction of a single finned tube on several cross sections before the tube (in the figure, x is the distance from the cross section to the center of the tube). As shown in the figure, for $x/d = -1.43$ the streamline begins to curve distinctly. For $x/d = -1.14$, a reflux region appears and then the gas velocity reduces to a very small value and a flow stagnant region is created in the slots between couples of fins from $x/d = -1.0$ to 0.0.

Fig. 6 shows the two-dimensional velocity vector of a particle in a finned tube; the stagnant and reflux regions are obvious. Fig. 7 shows the two-phase x-directional flow and the slip velocity distributions of a single finned tube along the flow direction. From $x/d = -2.0$ to $x/d = -1.0$ before the tube, the slip velocity is somewhat larger than zero because of the particle's inertia at the $-0.5 < y/d < 0.5$ section, and from $x/d = -1.0$ to $x/d = 0.0$, due to the effect of the stagnant regions, the slip velocity and the particle's velocity are nearly zero.

The measurement results illustrate, according to the above flow field, that most of the particles in the separator can be separated from the gas phase from the section $x/d = -1.43$ and enter the region between the two fins. Furthermore, the reflux region makes it possible that the rebounded particles can be dragged back into the region between the two fins.

Fig. 8 shows the gas turbulence intensity distribution of the single finned tube along the tube. At the entrance of the region between the two fins, the turbulence intensity is small, which prevents the particles in that region from escaping from it. In addition, the experimental results show that the largest value of the cross-section-mean turbulence intensity appears in the section $x/d = 3.0$ behind the tube.

The gas–solid turbulence intensity distribution when particles are put into the gas flow of a finned tube is shown in

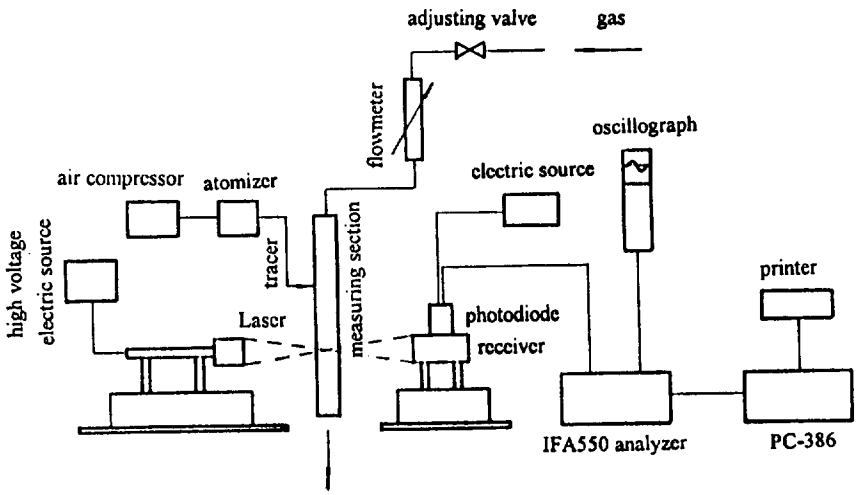

Fig. 2. Schematic diagram of the laser Doppler velocity measurement system.

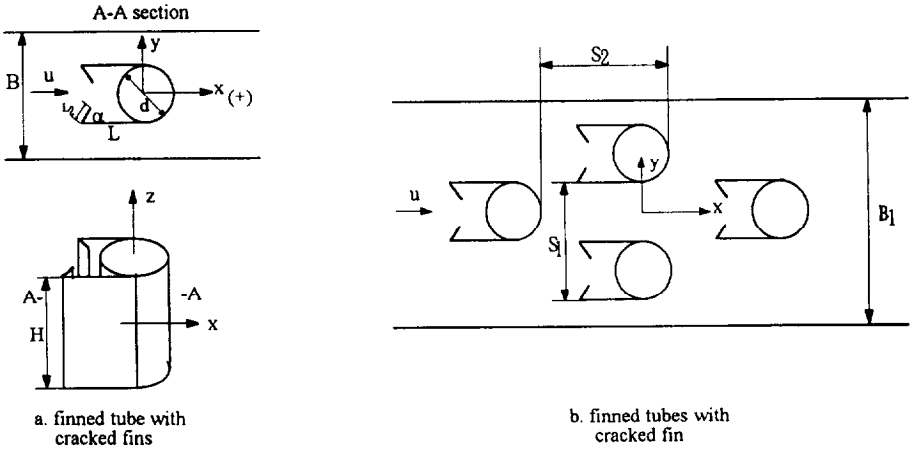

a. finned tube with cracked fins

b. finned tubes with cracked fin

Fig. 3. The coordinate systems of the measurement parts.

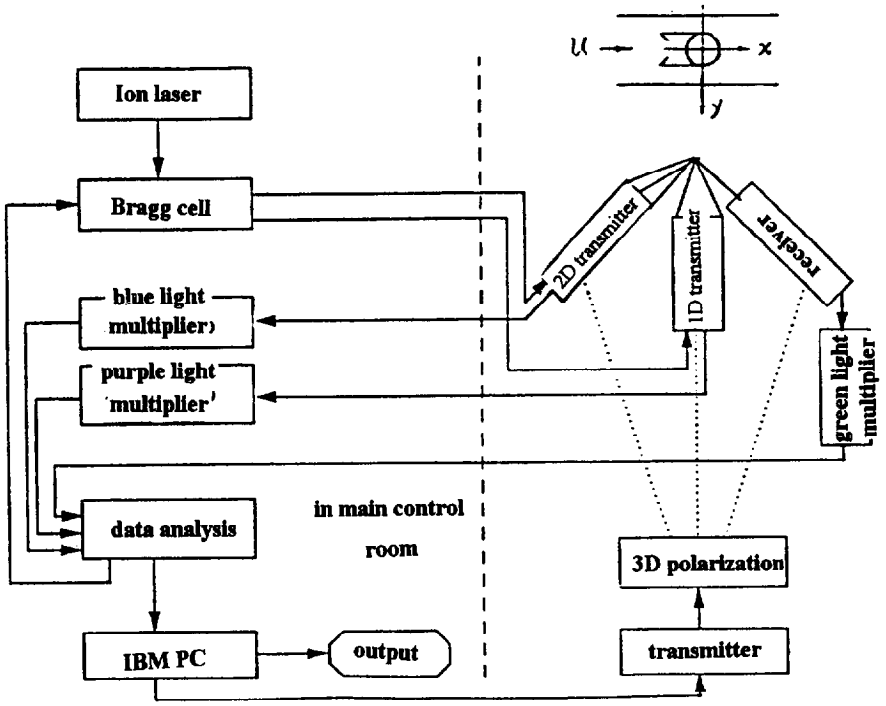

Fig. 4. Schematic diagram of the particle dynamics analyzer measurement system.

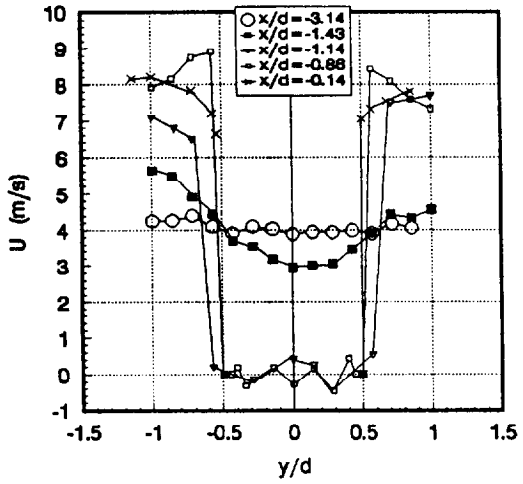

Fig. 5. Before-tube gas velocity distribution.

Fig. 9. From the figure, the gas turbulence intensity before the tube (up to $x/d = -1.0$) is nearly equivalent to that of the single tube flow, but larger than that of the single tube flow from $x/d = -1.0$. Before $x/d = -1.0$, the motion of the particles is uniform and has a small effect on the gas turbulence intensity. However, from $x/d = -1.0$, i.e. from the fins area, the gas turbulence intensity increases due to the particle's violent motion and the impact effects among the particles. Fig. 9 also shows that the particle turbulence intensity is higher than that of the gas phase before $x/d = 0.0$ because of the collision effects of the particles and lower than that of the gas phase after $x/d = 0.0$. From this section, due to the reflux flow and acceleration, the gas turbulence intensity is increased to a high value. Meanwhile the particle turbulence intensity does not follow the variation of the gas phase because the particle's inertia is large and the impact proba-

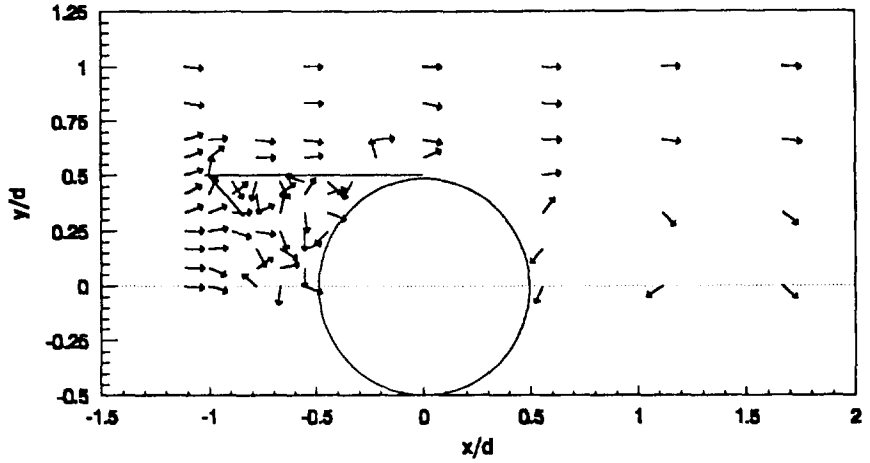

Fig. 6. Particle two-dimensional velocity vector.

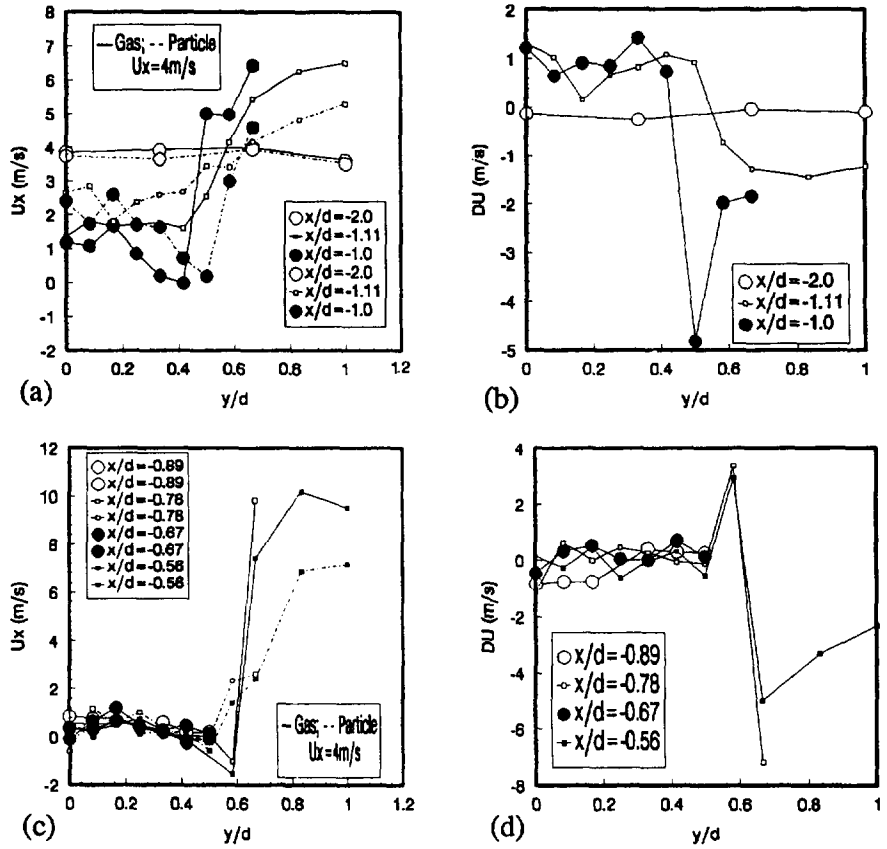

Fig. 7. Gas–solid two-phase flow and slip velocity distribution of a single finned tube. (a) Two-phase velocity distribution before the finned tube. (b) Gas–solid slip velocity distribution before the finned tube. (c) Two-phase velocity distribution between the fin's sections. (d) Gas–solid slip velocity distribution between the fin sections.

bility among particles decreases due to the low particle concentration at the back of the finned tube.

PDA measurement results also show that for two-phase flow the largest value of the cross-section-mean turbulence intensity appears at the section $x/d = 1.0$–1.5 behind the tube and not at $x/d = 3.0$ as for the single phase flow.

The effect of neighboring tubes on the flow field in the finned tubes separator has been studied by PDA. Four finned tubes arranged in three rows are placed vertically in a plexiglas measuring part with a square-cross-sectional area of 80×144 mm^2. The parallel and normal intervals are twice the diameter of the finned tube, 36 mm. The coordinate system is shown in Fig. 3.

Fig. 10 presents the particle velocity distributions in the normal direction along the finned tubes. Due to the effects of neighboring tubes, the particle reflux flow behind the first second row's tubes does not appear.

Fig. 11 shows the particle turbulence intensity distributions of the finned tubes at the front section before the tubes. In the figure, $x/d = -1.11$ is the front section of the second

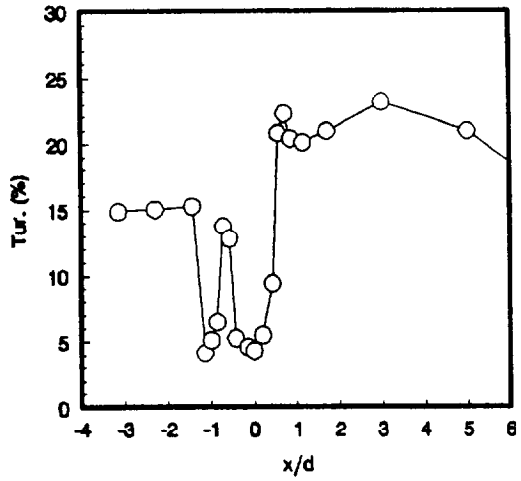

Fig. 8. Gas turbulence intensity distribution of a finned tube.

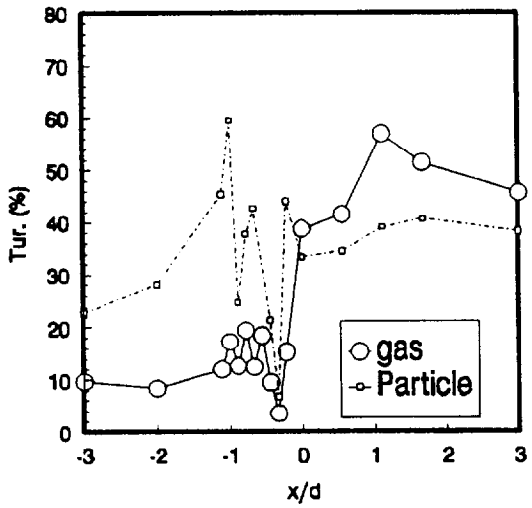

Fig. 9. Gas and particle turbulence intensity distribution of a single finned tube.

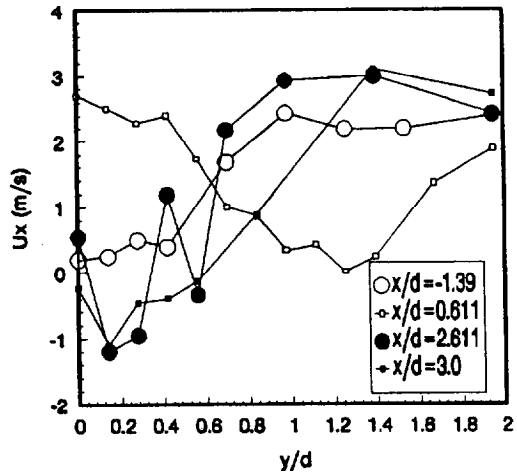

Fig. 10. Particle normal-directional velocity distribution along finned tubes.

tube row, $x/d=-3.11$ is that of the first tube row and $x/d=0.89$ is that of the third tube row. The dotted line in the figure represents the measurement results of the single tube flow. From the figure, the particle turbulence intensities

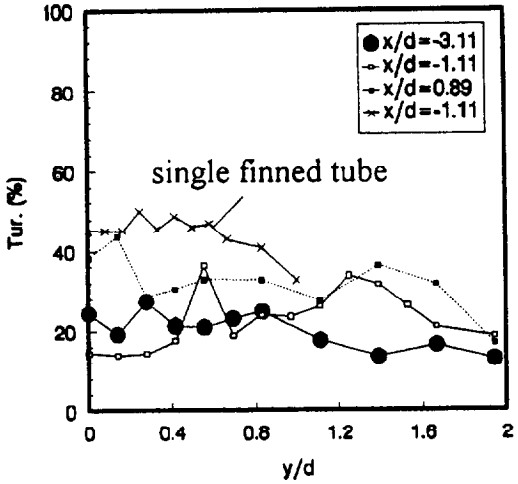

Fig. 11. Particle turbulence intensity distribution along finned tubes.

before the three tube rows increase with the tube row and all of them are lower than that of a single tube flow. This phenomenon is probably due to the flow stagnant and direction-guide effect of the latter tube row.

From the above, the LDV and PDA measurement results of the fluid dynamics characteristics of a finned tube and finned tubes show that a helpful flow structure is created in the finned tubes separator and lays the foundation of the following study.

3. Temperature distribution and heat transfer performance of a finned tube

Under high temperature conditions, the temperature of the fins is higher than that of the tubes. In order to avoid overly high temperatures in the fins, the fins must not be too long, thus relatively cheap steel can be employed for the fins. In this paper, the temperature distribution in a thin fin under hot conditions is calculated to find out a reasonable fin length [7].

Fig. 12 shows the heat flux through a fin (let the height of the fin, Z, be 1). For a cuboid whose length in the X-direction is dX, based on the heat flux balance of the cube and neglecting the radiation for the neighboring fins to simplify the problem, the following differential equation is obtained:

$$\lambda A_f \frac{d^2t}{dx^2} = \alpha_0 U(t-t_f) + \sigma\epsilon\left[\left(\frac{t+273}{100}\right)^4 - \left(\frac{t_f+273}{100}\right)^4\right] \quad (1)$$

with the boundary condition:

$$X=0, \qquad t=t_f$$

$$X=L, \quad -\lambda\left.\frac{dt}{dx}\right|_{X=L} = \alpha_0(t_L-t_f)$$

The convective coefficient α_0 for the tube surface is calculated from the following equation which is obtained from the heat transfer experimental results [7].

$$Nu_f = 0.0423Re_f^{0.7397} \quad (2)$$

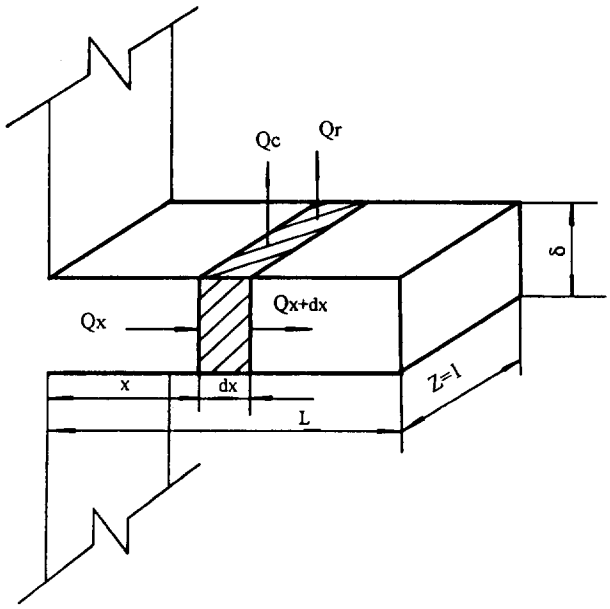

Fig. 12. Heat flux through the fin.

In Eq. (1), the fin emissivity ϵ is chosen to be 0.8. In Eq. (2), the influence of the solid loading on α_0 is not considered because the influence is very complex. In generally, α_0 will increase with solid loading so that it is safe if the influence of solid loading on α_0 is not taken into account.

After applying the finite-difference numerical method to solve Eq. (1), the following results are obtained. Curves (a) and (b) in Fig. 13 are the variations of the fin temperature with the tube wall temperature and the fin length, for which the gas temperature is 850 °C and the gas velocity is 6.6 m s^{-1}. In the calculation, the tube diameter is 35 mm. As can be seen in the figure, when the temperature of the tube wall is lower than 450 °C and the fin length is less than 45 mm, the highest temperature in the fin is lower than 790 °C. Hence heat-resisting steel can be employed.

Curves (c) and (d) in Fig. 13 show the variations of the temperature of the fin top with the temperature of the tube wall and the length of the fin when the gas temperature decreases to 550 °C. The curves indicate that when a finned tube is arranged in the intermediate temperature region, the highest temperature in the fin will be much lower than that shown in curves (a) and (b). Therefore the fin can be made of common steel.

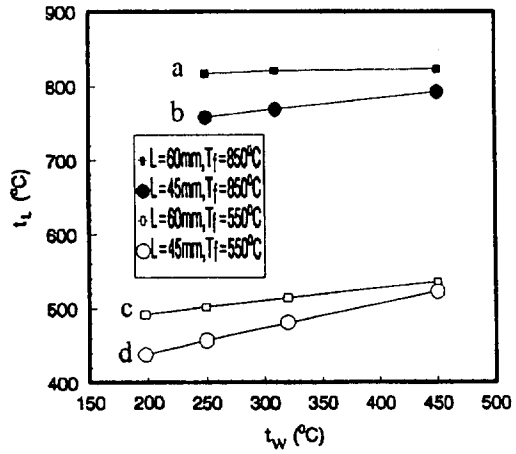

Fig. 13. Temperature of the fin top.

The fins can also enhance the heat transfer behavior of the finned tubes. Initial cold experiments have been carried out to study the heat transfer enhancing capacity of the finned tubes. The results show that when the gas velocity is between 3.3 and 10.0 m s^{-1}, the temperature of the outer wall of the tubes is 81 °C, the gas temperature is 23 °C, the fin length is 35 mm, and the heat transfer rate of a single finned tube is about 60% higher than that of a single bare tube.

4. Separation and pressure drop performance of the separator

4.1. Experimental apparatus and method

Fig. 14 shows a schematic diagram of the experimental apparatus. The size of the separator is $630 \times 360 \times 275$ mm^3 in length, width and height respectively. The solids are introduced into a Venturi tube from a hopper via a screw feeder. There is a long enough straight pipe (about 3.5 m long, 9.5 times the hydraulic diameter of the separator's cross section) between the Venturi tube and the separator to ensure that the velocity of the fed solids is as high as that of the gas. At most nine staggered rows of finned tubes with a diameter of 35 mm (for U-beams, the fin length is 40 mm) can be arranged in longitude and five columns can be arranged in latitude. The solid material is quartz sand whose density and bulk density are 2650 and 1550 kg m^{-3} respectively. The outer mean diameter of the sand is 260 μm. The particle size distribution is shown in Fig. 15.

The gas flow rate is measured by a rotameter. The feed and the separated particles are weighted by a precise balancer; the maximum deviation is 1%. The pressure drop of the separator is measured using a U-type glass column; the maximum deviation is 9.8 Pa.

The particle concentration is calculated from the following equation:

$$C = \frac{G_i}{Q\tau} \tag{3}$$

The separation efficiency can be determined by analyzing any two of the three material streams involved in the separation: the feed, the separated product and the unseparated fine product. The first two factors are adopted to determine the separation efficiency from the following equation:

$$\eta = \frac{G_s}{G_i} \times 100\% \tag{4}$$

It is useful to perform an uncertainty analysis for the separation performance tests. Leaving aside systematic errors, i.e. assuming perfect calibration of the instruments, the ran-

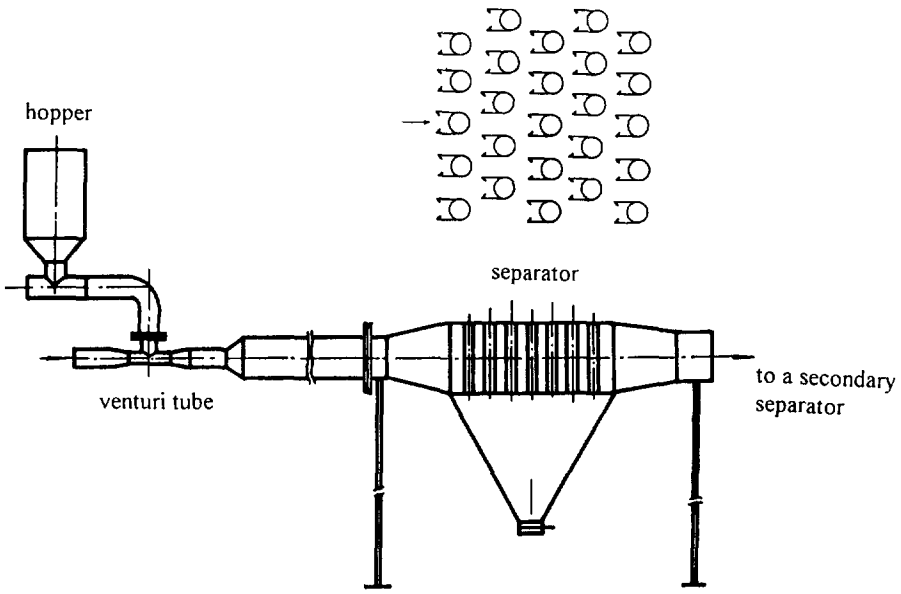

Fig. 14. Schematic diagram of the experimental set-up for the separator.

dom errors in all independent measured variables will be reflected in an error in the efficiency determined. The standard deviation of the efficiency can be calculated from the standard deviations of the feed G_i and the separated particles G_s using the following equation:

$$\sigma_\eta = \sqrt{\left(\frac{1}{G_s}\right)^2 \sigma_j^2 + \left(\frac{G_i}{G_s^2}\right)^2 \sigma_s^2} \quad (5)$$

In Eq. (5), it is acceptable that G_i and G_s are made equal to 1 kg because all of the G_i and G_s in the test runs are larger than this value. According to error theory, the standard deviations σ_j and σ_s for G_i and G_s respectively are calculated by the maximum deviation, i.e. a third of the maximum deviation. Based on Eq. (5) and the above parameters, the standard deviation of the efficiency is about 0.47%.

4.2. Results and discussion

The following parameters have great effects on the separation efficiency of the separator: normal and parallel tubes interval, fin length, number of the tube row, particle diameter, gas velocity and particle concentration. The results are presented to show the effect of these parameters and the pressure drop performance of the separator.

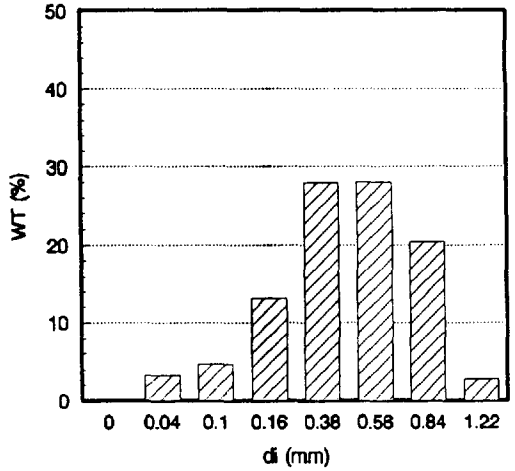

Fig. 15. Quartz sand size distribution.

4.2.1. Effect of fin length

The study of the fluid dynamics characteristics revealed that when the fin is not long enough, the particles may be easily bounced back to the main flow which leads to a low separation efficiency, so the fin length should be long enough. However, due to the temperature limit of the fin material, fins that are too long are not feasible because of the temperature distribution of the fin as shown in Fig. 13. It is recommended to choose $L/d = 1.0$, where L is the fin length and d is the diameter of the tube.

4.2.2. Effect of tubes interval

The variation of tube interval affects the separation remarkably. Let the parallel interval of the tubes be S_1/d, the normal interval of the tubes be S_2/d. Fig. 16 shows the effect of S_1/d on the separation efficiency. As shown in the figure, S_1/d has an optimum value of about 2.0. When S_1/d is too small, the suspension velocity between the tubes increases, thus leading to an increase of the entrainment ability of the main flow. Therefore the separation efficiency decreases with the increase of the re-entrainment. When S_1/d is larger than 2.0, the increase of S_1/d means that the number of the tubes in each row of the separator may decrease, so S_1/d must not be too large. Fig. 17 shows the effect of S_2/d on the separation efficiency; the efficiency decreases with S_2/d. Since the tubes are welded with fins and sufficient flow space between the tubes and the fins is needed, a value of S_2/d that is too small is not advisable. According to the results, $S_2/d = 2.0$ is reasonable.

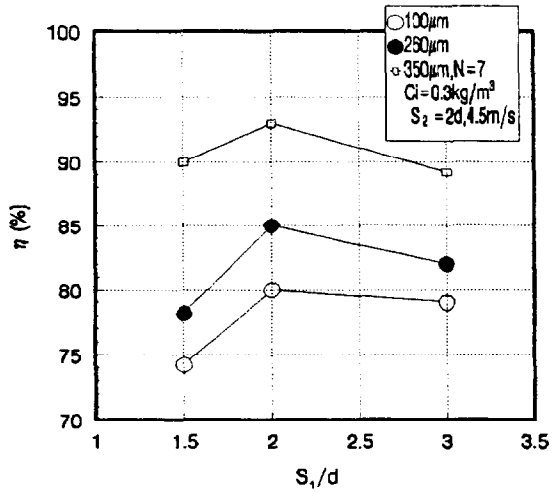

Fig. 16. Effect of parallel interval on separation efficiency.

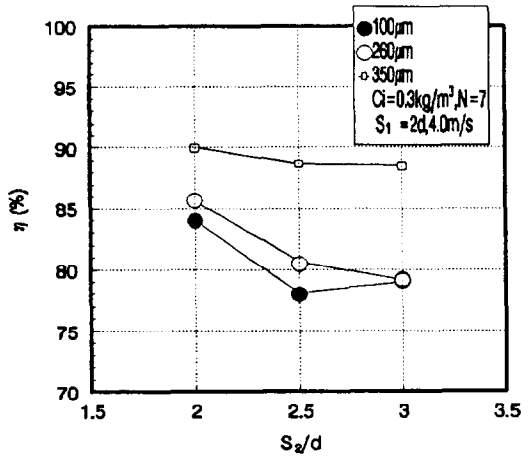

Fig. 17. Effect of normal interval on separation efficiency.

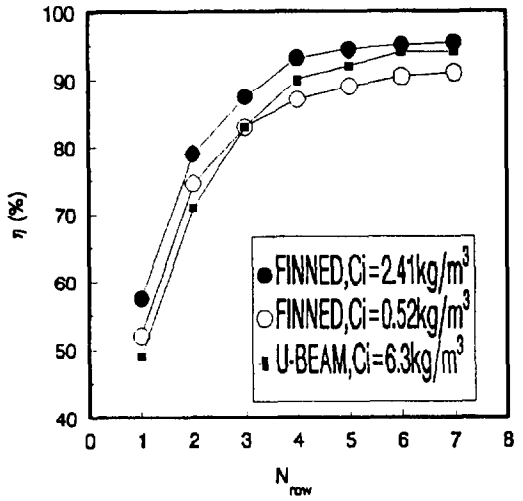

Fig. 18. Effect of number of tube rows on separation efficiency.

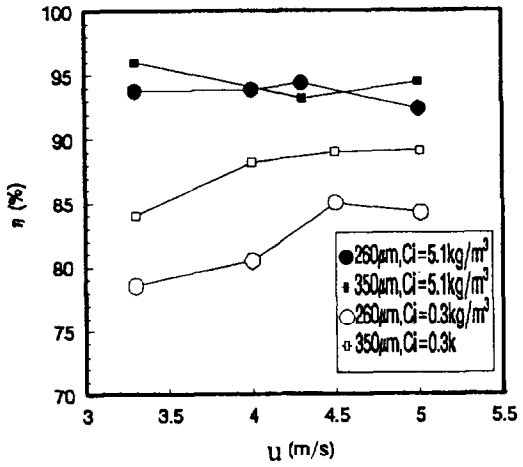

Fig. 19. Effect of gas velocity on separation efficiency.

4.2.3. Effect of the number of tube rows

Let the number of tube rows be N. Fig. 18 shows the effect of N on the separation efficiency. The figure shows that with increasing N the separation efficiency increases, but most of the separated particles are captured by the first four rows. The amount of particles captured by the first four rows reaches up to 90–95% of the total amount captured by seven rows. When the inlet particle concentration increases, this percentage will increase slightly. Therefore four or five rows are enough for a certain efficiency requirement. If there are too many rows, the increase of the separation efficiency will not be significant while the pressure drop may increase rapidly.

In Fig. 18, the result of the U-beams separator based on our experiments is also given. The trend of increasing efficiency with tube rows, and the total efficiency, are nearly the same as that of the finned tubes separator.

4.2.4. Effect of gas velocity

In impingement separators, the particle inertia increases with suspension velocity, thus making the particles more easily separable from the main flow. On the other hand, the entrainment capacity of the main flow, which depends directly on the square root of the particle diameter, increases with the gas velocity. This effect will lead to a decrease of the separation efficiency. Due to these two effects, there is an optimum value of the gas velocity. For the finned tubes impact separator, the gas velocity is based on the cross-section ($A = 360 \times 275$ mm^2) of the separator. Fig. 19 presents the effect of the gas velocity. It can be concluded that at a low inlet particle concentration the separation efficiency reaches its highest value when the velocity is about 4.5 m s^{-1}, while at a high inlet particle concentration the gas velocity has almost no effect on the separation efficiency. Therefore a finned tubes impact separator used in CFBB may have good separation performance even if it operates at low gas velocity. Considering the pressure drop of the separator, a gas velocity of about 4.0 m s^{-1} is appropriate.

4.2.5. Effect of inlet particle concentration and diameter

Much has been written on the effect of the inlet particle concentration on the separation efficiency [8–11]. In most of these publications, it is reported that if the inlet particle concentration is low, the separation efficiency increases with increasing inlet particle concentration. Some researchers have found that if the inlet particle concentration is very high the

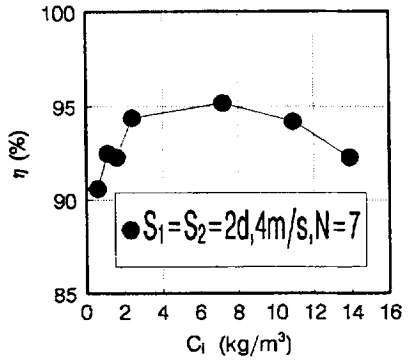

Fig. 20. Effect of inlet particle concentration on separation efficiency.

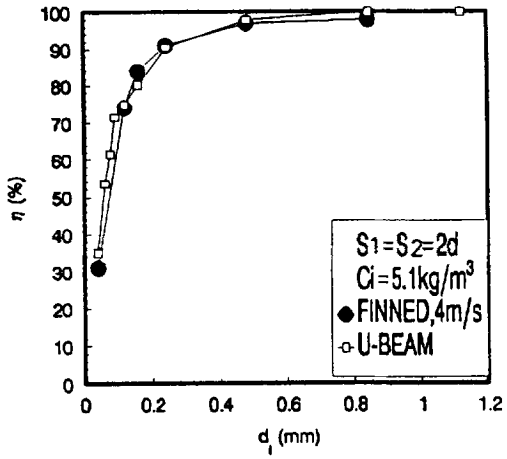

Fig. 21. Effect of inlet particle diameter on separation efficiency.

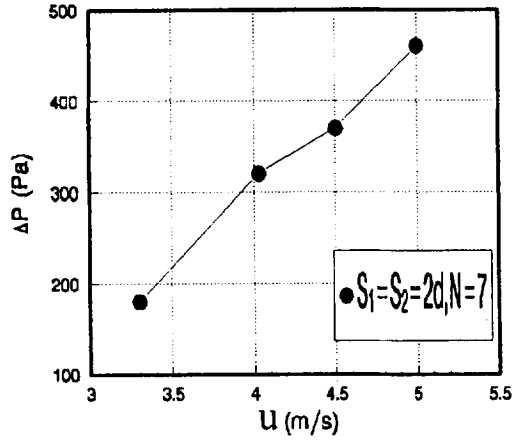

Fig. 22. Effect of gas velocity on pressure drop.

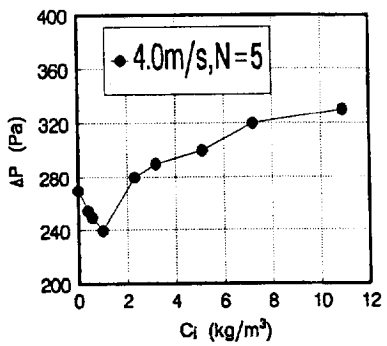

Fig. 23. Effect of inlet particle concentration on pressure drop.

separation efficiency may decrease. In this paper, the variation of the separation efficiency with the inlet concentration ranging from 0 to 14 kg m^{-3} has been studied. Fig. 20 shows the relationship between the separation efficiency and the inlet particle concentration. As shown in the figure, the separation efficiency increases with the inlet concentration before it reaches its highest value (95.4% with an inlet particle concentration of 7.0 kg m^{-3}), beyond which it falls off.

The separation efficiency increases with the particle diameter because the particle inertia increases with its diameter. According to the experimental results shown in Fig. 21 the cut size of this separator is about 60 μm.

According to our experimental results, the grade efficiency of the U-beams separator is also shown in the figure and the cut size is about the same as that of the finned tubes separator.

4.2.6. *Pressure drop performance*

The pressure drop of the separator is low and increases with the number of tube rows. Therefore it is better not to use too many rows in order to obtain a low pressure drop and a high enough separation efficiency. Fig. 22 shows the effect of the gas velocity on the pressure drop. The pressure drop increases with increasing gas velocity.

Many researchers have shown much interest in the effect of the inlet particle concentration on the pressure drop of gas–solid separators [9,10,12]. Most carried out their experimental study under low particle concentration conditions (maximum value up to several hundreds of g m^{-3}) and found that with the increase of the particle concentration, the pressure drop may decrease. In this paper, the experiments cover a wide range of inlet particle concentrations. The results (see Fig. 23) show that at a low inlet particle concentration the profile of the pressure drop is similar to that reported by other researchers, while at a high inlet particle concentration (higher than 1.0 kg m^{-3}), the pressure drop may increase with the increase of the inlet particle concentration.

However, when the inlet particle concentration is high enough, the increase of the pressure drop will be less.

Based on the experimental results, two empirical correlations are presented. Eq. (6) is the pressure drop equation of the pure gas phase and the other is that of a gas–solid suspension. Compared to the experimental data, the maximum error of these equations is less than 3%.

$$\Delta P_g = 6.34 N^{0.78} \frac{\rho W^2}{2} \tag{6}$$

$$\Delta P_{gs} = \begin{cases} 6.34 N^{0.78} \dfrac{\rho W^2}{2} e^{-0.110\left(\frac{C_i}{C_{cr}}\right)} & C_i < C_{cr} = 1.0 \text{ kg m}^{-3} \\ 6.63 N^{0.78} \dfrac{\rho W^2}{2} \left(\dfrac{C_i}{C_{cr}}\right)^{0.139} & C_i > C_{cr} = 1.0 \text{ kg m}^{-3} \end{cases} \tag{7}$$

5. Wear of the separator

Since the separation targets are welded on the tubes, it is more important for this separator to protect the tubes from being worn. However, at low gas velocity (about 4.0 m s^{-1}) and high inlet particle concentration, wear of the tubes will be reduced because the particles must pass through a dense particle region before impacting on the tubes. The site experimental results of Studsvik's U-beams separator have verified the above point of view [2]. To prevent contingent serious wear of the tubes, a heat treatment such as carbonization or boronization can be used for the fins and the front of the first two rows to increase their wear-resisting capacity.

6. Conclusion

The flow structure of the two-phase flow of finned tubes is measured showing the good fluid dynamics characteristics of the finned tubes separator. The temperature in a fin is calculated and initial heat transfer experiments indicate that the fins may lead to a ~60% increase of the heat transfer rate. Based on a series of experiments, the optimum values of the following parameters are presented: fin length, parallel and normal interval between the tubes, suspension velocity, number of tube rows. The effect of the inlet particle concentration and particle diameter on the separation efficiency and pressure drop performance of the separator are shown.

The above results show that the finned tubes impact gas–solid separator presented in this paper has advantages such as high efficiency, low pressure drop and more compact structure, it can enhance heat transfer as well and the fins can be made of common steel or heat-resisting steel contrary to other impact separators such as the U-beams separator. In brief, this separator is very suitable for circulating fluidized bed boilers (CFBB) with a high furnace outlet particle concentration.

7. Nomenclature

A	cross-sectional area of the separator	mm^2
A_f	cross-sectional area of the cuboid (see Eq. (1))	m^2
C_{cr}	inlet particle concentration with the lowest pressure drop	kg m^{-3}
C_i	inlet particle concentration	kg m^{-3}
D_i	inlet particle diameter	mm
d	tube diameter	mm
G_i	particle quantity fed during given time	kg
G_s	particle quantity separated during given time	kg
L	fin length	mm
N	number of tube rows	
Nu_f	Nusselt number (see Eq. (2))	
Q	gas flow rate	m^3 s^{-1}
Q_c	convective heat flux (see Fig. 12)	W
Q_r	radiate heat flux (see Fig. 12)	W
Q_x	conductive heat flux at location x (see Fig. 12)	W
Re_f	Reynolds number based on d	
S_1	parallel tubes interval	mm
S_2	normal tubes interval	mm
Tur	turbulence intensity	%
T_w	temperature of tube wall	°C
t	temperature of the cuboid (see Eq. (1))	°C
t_f	temperature of gas	°C
t_L	temperature of fin top	°C
U	inlet velocity (see Fig. 5)	m s^{-1}
U	circumference of the cross section (see Eq. (1))	m
W	gas velocity	m s^{-1}
wt	weight percent of test particles	%
ΔP_g	pressure drop of the separator (pure gas phase)	Pa
ΔP_{gs}	pressure drop of the separator (gas–solid suspension)	Pa
α_0	convection coefficient	W m^{-2} K^{-1}
λ	thermal conductivity of the fin	W m^{-1} K^{-1}
ϵ	emissivity of the fin	
ρ	gas density	kg m^{-3}
σ	Stefan–Boltzman constant	W m^{-2} K^{-4}
σ_η	the standard deviation of the separation efficiency	
σ_j	the standard deviation of the feed particles	
σ_s	the standard deviation of the separated particles	
τ	given time (see Eq. (3))	s
η	separation efficiency	%

References

[1] S.L. Darling, H. Beisswenger and A. Vechsler, The Lurgi/combustion engineering circulating fluidized bed boiler—design and operation, in: Proc. of the 1st International Conference on CFB, 1985, pp. 297–308.

[2] R.F. Johns and R.E. Wascher, Design and construction of a wood-fired circulating fluidized bed boiler, in: Proc. of the 9th International Conference on FBC, 1987, pp. 385–391.

[3] F. Belin and T.J. Flynn, Circulating fluidized bed boilers solids system with in-furnace particle separator, in: Proc. of the 11th International Conference on FBC, 1991, pp. 385–391.

[4] J. Makansi, Special report for fluidized bed boilers, power, March 1991, pp. 15–21.

[5] Zhang Yongzhao, Li Yingtang, Zhang Ximing, Jing Pingan, Duan Jianzhong, Bao Bongwen and Wang Ganghua, Experimental study of a slotted tube impact separator, Chinese J. Power Eng. 6 (1989) 9–13.

[6] Chinese Patent, No. 93.235633.8, February 1994.
[7] Li Xiaodong, Experimental and Theoretical Study of Gas–Solid Separation Technologies for Circulating Fluidized Beds, PhD Thesis, Zhejiang University, 1994.
[8] M. Trefz, E. Muschelknautz, Extended cyclone theory for gas flows with high solids concentration, Chem. Eng. Technol. 16 (1993) 153–160.
[9] L. Svarovsky (Ed.), Handbook of Powder Technology, vol. 3, Elsevier, Amsterdam, 1981.
[10] A.C. Stern, K.J. Caplan and P.D. Bush, Cyclone Dust Collector, API Report, 1955.
[11] W. Licht, Air Pollution Control Engineering—Basic Calculation for Particulate Collection, 1980.
[12] A. Ogawa, Separation of Particles from Air and Gases, CRC Press, 1984.